







Deciphering sources and processing of dissolved black carbon in coastal seas

Hongyan Bao ^{1,*} Jutta Niggemann ² Moge Du,¹ Weiqiang Zhao,¹ Dekun Huang ³ Yuanbi Yi,⁴ Jin-Yu Terence Yang ¹ Thorsten Dittmar ^{2,5} Shuh-Ji Kao ^{1,6}

¹State Key Laboratory of Marine Environmental Science, College of Ocean and Earth Sciences, Xiamen University, Xiamen, China

²Research Group for Marine Geochemistry (ICBM-MPI Bridging Group), Institute for Chemistry and Biology of the Marine Environment, University of Oldenburg, Oldenburg, Germany

³Third Institute of Oceanography, Ministry of Natural Resources, Xiamen, China

⁴Department of Ocean Science and Center for Ocean Research in Hong Kong and Macau, The Hong Kong University of Science and Technology, Hong Kong SAR, China

⁵Helmholtz Institute for Functional Marine Biodiversity (HIFMB) at the University of Oldenburg, Oldenburg, Germany

⁶State Key Laboratory of Marine Resource Utilization in the South China Sea, School of Marine Science and Engineering, Hainan University, Haikou, Hainan, China

Abstract

Dissolved black carbon (DBC) is the largest known slow-cycling organic carbon pool in the ocean; yet, its sources and processing in the coastal seas remain poorly understood. To address this knowledge gap, we conducted a study in the East China Sea and South Yellow Sea to quantify and molecularly characterize DBC using benzene polycarboxylic acids (DBC_{BPCA}) and ultra-high resolution mass spectrometry (DBC_{FT}), respectively. The concentration of DBC_{BPCA} was 0.70–1.9 μmol C L⁻¹ and exhibited a significant negative correlation with salinity. Significant correlations were also observed between salinity and molecular characters (oxygen-to-carbon ratio; double bond equivalent; molecular weight) of DBC_{FT}. These findings collectively suggest that mixing processes primarily control the concentration and composition of DBC. A two-end-member mixing model revealed that riverine input and offshore water contributed ~ 22% and 63%, respectively, to the DBC_{BPCA} in the study region. Additionally, atmospheric deposition and potentially other unidentified sources contributed at least ~ 15% DBC_{BPCA}, assuming no removal. Furthermore, ~ 70% of DBC_{FT} in the coastal seawater could be found in the river water, and aerosols, which was in line with the information from DBC_{BPCA}. Our study provides the first comprehensive assessment of both the sources and influential processes of DBC in coastal seas, highlighting the importance of additional sources, such as atmospheric deposition, and emphasizing the need to identify previously unknown sources of DBC.

The incomplete combustion of biomass and fossil fuel results in the release of a continuum of black carbon (BC; Kuo et al. 2011; Liu et al. 2021; Schmidt and Noack 2000). Part of the BC is transported to the oceans in a dissolved form known as dissolved BC (DBC) through various pathways (Bao

et al. 2017; Jaffe et al. 2013; Jones et al. 2020). DBC constitutes ~ 2% of oceanic dissolved organic carbon (DOC) and is characterized by a depletion in radiocarbon (Ziolkowski and Druffel 2010). It represents the largest known pool of refractory DOC in the ocean (Dittmar and Paeng 2009). Therefore, it is crucial to understand the sources and fate of DBC in the ocean for a comprehensive understanding of the global carbon budget.

Each year, ~ 18–27 Tg of DBC is delivered to the ocean through riverine discharge, while atmospheric deposition contributes around 1.8 Tg (Jaffe et al. 2013; Bao et al. 2017; Jones et al. 2020). Tidal pumping from coastal wetlands and hydrothermal vents are also significant regional sources of DBC (Dittmar et al. 2012; Yamashita et al. 2023), although their total flux on a global scale has not been well quantified.

*Correspondence: baohy@xmu.edu.cn

Additional Supporting Information may be found in the online version of this article.

Author Contribution Statement: H.B., J.N., T.D., and S.K. conceptualized the study. H.B. collected the samples, did the chemical analysis under the guidance of J.N., performed the data analysis and wrote the first draft of the manuscript. W.Z., Y.Y., and D.H. helped to prepare the figures. J.Y. investigated the main water masses. M.D. performed the end-member model calculation. S.K. and H.B. acquired funding. All the authors commented and revised the manuscript.

However, the observed ~ 6‰ difference in the stable carbon isotope values between riverine and oceanic DBC contradicts the known sources of DBC in the ocean (Wagner et al. 2019a), highlighting the need for a better understanding of the sources and processes involved, particularly in the coastal regions (Wagner et al. 2019a; Coppola et al. 2022). Previous studies have been conducted in various ocean basins, such as the South China Sea (Fang et al. 2017), Bohai Sea (Fang et al. 2021b), and Bering Sea (Fang et al. 2021c). However, the lack of molecular information hinders our understanding of how DBC is modified and how its composition is linked to its sources and processes. Additionally, most studies have relied on top-down flux estimations to assess the contributions from different transport pathways. Nevertheless, it remains unconfirmed how changes in DBC concentration and composition in coastal seas respond to the various input sources.

Currently, no single method can fully capture the entire spectrum of BC due to its complex nature (Wagner et al. 2018, 2021). The benzenepolycarboxylic acids (BPCA) method is commonly used to quantify the specific fraction of DBC (noted as DBC_{BPCA}) in natural dissolved organic matter (DOM) obtained from rivers, oceans, and atmospheric deposition (Ziolkowski and Druffel 2010; Jaffe et al. 2013; Bao et al. 2017; Jones et al., 2019, 2020; Geng et al. 2021; Wagner et al. 2021). Additionally, Fourier transforms ion cyclotron resonance mass spectrometry (FT-ICR-MS), a state-of-the-art technique with exceptional resolution, allows for detailed molecular characterization of DBC (noted as DBC_{FT}) (Chen et al. 2022; Qi et al. 2022). This technique has proven to be valuable in studying the composition of DBC in various environments (Bao et al. 2017; Roebuck et al. 2017; Coppola et al. 2019; Zhao et al. 2023). DBC_{BPCA} and DBC_{FT} are used to characterize the fraction of BC that forms at intermediate temperature and is relatively resistant to biodegradation (Wagner et al. 2018). Thus, the combination of FT-ICR-MS and BPCA methods has the potential to elucidate the sources, molecular character, and processing of the bio-refractory fraction of DBC in the coastal region.

The DBC_{BPCA} can be removed from the water column through processes such as photodegradation and particle sorption (Dittmar and Paeng 2009; Stubbins et al. 2012; Coppola et al. 2014). While some studies have observed biodegradation of DBC derived from biochar (Norwood et al. 2013; Qi et al. 2020), the DBC_{BPCA} fraction from both fresh and photodegraded biochar has been found to be resistant to biodegradation, with only ~ 5% degradation occurring over a period of 66 d (Bostick et al. 2021). This resistance to biodegradation aligns with the distribution of DBC_{BPCA} in the global oceans (Dittmar and Paeng 2009; Wagner et al. 2021). Particle sorption has been proposed as the primary process for removing DBC_{BPCA} in the open ocean (Yamashita et al. 2022). A previous study in the Arctic region indicated that the deposition of particulate BC in the ocean exceeded the input (Fang et al. 2016), suggesting an additional source of particulate BC, likely resulting from scavenging from the dissolved phase.

Condensed aromatics are believed to preferentially adsorb onto particles, leaving fewer condensed aromatic structures in the water column (Coppola and Druffel 2016; Coppola et al. 2014; Yamashita et al. 2022). Thus, a more detailed characterization of the molecular composition of DBC can help to understand its sources and influencing processes better.

In this study, we conducted research in the East China Sea and the South Yellow Sea during the spring season, which is known for its significant atmospheric deposition (Bao et al. 2017, 2022). The East China Sea is home to one of the largest continental shelves globally, which supports a complex circulation system that potentially facilitates the biogeochemical processing of DOM. During the cruise, we observed a clear decrease in atmospheric deposition from the South Yellow Sea to the East China Sea. This makes the study area ideal for investigating the impact of atmospheric deposition on the distribution of dissolved BC (DBC; Bao et al. 2017). To determine the sources of DBC in seawater, we compared its molecular composition with samples collected from rivers and aerosols.

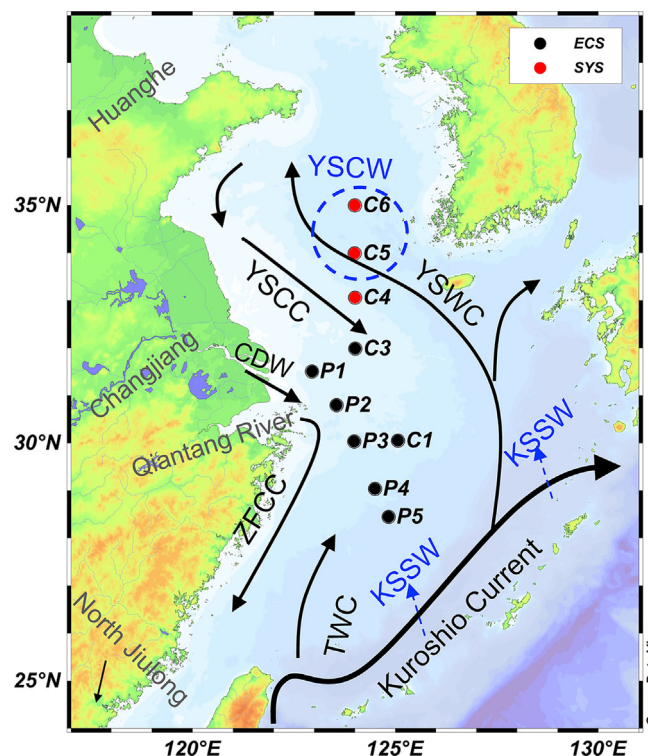


Fig. 1. Sampling locations and major water masses in the study area. Red and black dots denote stations in the South Yellow Sea (SYS) and East China Sea (ECS), respectively. The black arrows indicate the surface current, and the blue dash lines indicate the subsurface current. The information for main water masses in spring was from previous studies (Chen 2009). YSWC, Yellow Sea warm current; YSCC, Yellow Sea coastal current; YSCW, Yellow Sea cold water; ZFCC, Zhejiang-Fujian coastal current; CDW, Changjiang dilute water; TWC, Taiwan warm current; KSSW, Kuroshio subsurface water. This figure was drawn by ocean data view software (Schlitzer 2023).

The aerosol samples ($n = 46$) were collected during the same cruise as the seawater samples, and the DBC data were obtained from our previous studies (Bao et al. 2017; Bao et al. 2018; Fig. 1). The riverine samples ($n = 18$) were collected from the North Jiulong River, which flows into the East China Sea and covers a complete hydrograph (Bao et al. 2019). The objectives of our study were: (1) to characterize the molecular composition of DBC in the coastal seas; (2) to infer the sources and processes affecting the concentration and composition of DBC.

Materials and methods

Study area

The primary source of freshwater in the region is the Changjiang, which contributes $\sim 80\%$ ($900 \text{ km}^3 \text{ yr}^{-1}$) of the total freshwater input. Other rivers, such as the Huanghe and Qiantang Jiang, located along the east coast of China, account for the remaining 20% of freshwater discharge into the East China Sea and the Yellow Sea (Milliman and Farnsworth 2011). Although the Huanghe does not directly discharge into the Yellow Sea, it is still a significant contributor of freshwater to the area (Hwang et al. 2014).

The East China Sea is characterized by several major water masses. These include the Changjiang Dilution Water (with a specific salinity of < 31.00), and the Zhejiang-Fujian Coastal Currents, which flow southward along the coast. In addition, the warm and saline Taiwan Warm Current and the Kuroshio Current flow northward (Chen 2009; Fig. 1). In the spring, specific water masses in the South Yellow Sea include the Yellow Sea Cold Water, the Yellow Sea Coastal Current, and the northward Yellow Sea Warm Current, which is warmer and saltier (Fig. 1). While there is ongoing debate regarding the formation mechanisms of the Yellow Sea Warm Current, it is widely accepted that it originates from the Pacific Ocean as a branch of the Kuroshio Current (Liu et al. 2017; Lian et al. 2022).

Field sampling

A total of 10 stations were investigated in the South Yellow Sea and the East China Sea onboard R/V Dong Fang Hong 2 (Fig. 1). The stations were divided into two sections: P section, consisting of stations P1–P5, and C section, consisting of stations C1, C3–C6. The P section was sampled in early April 2015, while the C section was sampled in early May 2015. Water samples were collected using Niskin bottles attached to a conductivity, temperature, and depth (CTD) system. The CTD instrument recorded the depth, salinity, and water temperature. The water depth at each station ranged from 30 m to 104 m, and samples were taken from specific water layers, including the surface (5 m), chlorophyll max, middle layer (~ 10 –30 m), and near-bottom layer (5 m above the sea floor). The temperature differences between the in situ measurements (determined by CTD) and the potential temperature (in situ temperature corrected by depth) for all samples were $< 0.02^\circ\text{C}$, so the in situ temperature was used for analysis.

For each sample, 1 L water was first collected and filtered through 47 mm GF/F filters (pre-combusted at 450°C). DOC samples were sealed in pre-combusted (450°C for 5 h) glass ampoules. Filtered water samples for DBC_{BPCA} and Fourier transform ion cyclotron resonance mass spectrometry (FT-ICR-MS) analysis were immediately acidified to $\text{pH} = 2$ by adding hydrochloric acid (32%, Merck) and concentrated using solid phase-extraction (SPE) with PPL cartridges (500 mg, Agilent, USA) onboard (Dittmar et al. 2008). The cartridges were then dried by high purity N_2 on board and stored at -20°C until further processing and laboratory analysis. The sampling and processing methods for the river samples can be found in Bao et al. (2019).

Chemical analysis

The concentration of DOC was measured using a total organic carbon (TOC) analyzer (Shimadzu TOC VCPH) at Xiamen University. To ensure the accuracy of the data, reference samples of deep seawater from the Sargasso Sea (obtained from Dr. D.A. Hansell's lab at the University of Miami, FL, USA) were used for verification. The average analytical error, determined from duplicate measurements, was found to be $< 10\%$.

The concentrations of DBC were determined using (BPCA) method, as described by Stubbins et al. (2012) at Oldenburg University. This specific fraction of DBC is referred to as DBC_{BPCA}. Upon nitric oxidation, a series of BPCAs are released. The total concentration of DBC was calculated using a power-function relation between the most reliably quantified benzenepentacarboxylic acid (B5) and benzenhexacarboxylic acid (B6) and the total DBC concentration generated based on a set of 351 samples. The ratio of B6 to B5 (B6/B5) can be utilized as an indicator for molecular condensation of DBC, which typically decreases during photo-degradation (Stubbins et al. 2012). For quality control of the analytical procedure, a natural aquatic organic matter (NOM) reference sample (Suwannee River NOM, reference #2R101N) from the International Humic Substance Society (IHSS) was used. The standard deviation (SD) of DBC_{BPCA} concentrations and B6/B5 ratio, based on replicate measurements of the IHSS reference sample, were found to be less than 3% and 2%, respectively. Details of the processing method for riverine and aerosol samples can be found in previous studies (Bao et al. 2018, 2019).

For FT-ICR-MS analysis, the solid phase extractable DOC (SPE-DOC) sample was diluted with ultrapure water (18.2 M Ω) and methanol to achieve a methanol-to-water ratio of 1:1 and a final carbon concentration of 10 mg L^{-1} . Ultra-high-resolution mass spectral analysis was performed on a solarix (Bruker Daltonic, Germany) FT-ICR-MS equipped with a 15 Tesla magnet at Oldenburg University. The experimental procedure was described by Seidel et al. (2014). Samples were ionized in the negative mode in an electrospray source (ESI, Apollo ion source, Bruker Daltonic GmbH Bremen, Germany). A total of 500 scans were accumulated in the mass range of 150–2000 Da for each

sample. The acquired spectra were calibrated using an internal calibration list and the Bruker Daltonics data analysis software package. To ensure instrument performance, a deep seawater reference sample collected from the North Pacific Ocean (700 m, NEqPIW, www.icbm.de/en/ds-dom) was analyzed daily. Molecular formulae containing the elements C, H, O, N, S, and P were assigned using previously published criteria with a mass tolerance of < 0.5 ppm for seawater and aerosols (Koch et al. 2007), and using the ICBM- OCEAN (a server-based tool) with an error tolerance of < 0.5 ppm for river water (Merder et al. 2020). Only peaks with a signal-to-noise (S/N) ratio of 5 or higher, detected in at least two samples, were considered for further analysis. Peaks in blank samples with S/N larger than 20 were removed from all the samples. The reconstructed mass spectrum of the surface and bottom layers of P5 exhibited a non-Gaussian distribution, as shown in Supporting Information Fig. S1. This suggests possible contamination during sample processing. Consequently, the DBC_{FT} and DBC_{BPCA} data of surface and bottom layers of P5 were excluded from further analysis.

The modified aromaticity index (AI_{mod}) was calculated for each formula based on its elemental composition following the equation described in Koch and Dittmar (2016). Molecular formulas with an AI_{mod} > 0.66 are considered to be polycyclic aromatics (PCAs), which is indicative of DBC (Koch and Dittmar 2006; Seidel et al. 2015; Merder et al. 2020). These PCAs were denoted as DBC_{FT}. The number of DBC_{FT} in the NEqPIW sample was 27 ± 5 (n = 25), demonstrating the reliable reproducibility of our measurements. The nominal oxidation state of carbon (NOSC) and double bond equivalent (DBE) were calculated according to a previous study (Riedel et al. 2012). The NOSC increases with greater polarity, while the DBE value increases with higher degrees of unsaturation (Riedel et al. 2012). To represent the intensity-weighted average values, the parameters were suffixed with “wa.” For instance, the intensity-weighted average H/C ratio was denoted as H/C_{wa}.

End-member mixing model

In the study region, the primary source of freshwater input is derived from riverine discharge. Simultaneously, the Taiwan Warm Current and Kuroshio Current transport the main saline offshore water from the Pacific Ocean. Therefore, the relative contribution of riverine and offshore water to the study region was determined by assessing the salinity balance using the following equations:

$$S_{\text{sample}} = S_{E1} \times f_{E1} + S_{E2} \times f_{E2} \quad (1)$$

$$1 = f_{E1} + f_{E2} \quad (2)$$

where sample, E1 and E2 represent river and offshore end-member, respectively; f and S are the relative contribution and salinity, respectively.

The expected DBC_{BPCA} (DBC_{exp}) from the mixing and the difference between observed DBC_{BPCA} and DBC_{exp} (noted as ΔDBC) was then estimated by the following equations:

$$\text{DBC}_{\text{exp}} = \text{DBC}_{E1} \times f_{E1} + \text{DBC}_{E2} \times f_{E2} \quad (3)$$

$$\Delta\text{DBC} = \text{DBC}_{\text{BPCA}} - \text{DBC}_{\text{exp}} \quad (4)$$

A positive value of ΔDBC indicates an input of DBC, while a negative value indicates its removal. The contribution of each end-member to the DBC_{BPCA} of each sample was estimated as follows:

$$f_{\text{DBC}_{Ei}} = \text{DBC}_{Ei} \times f_{Ei} / \text{DBC}_{\text{BPCA}} \quad (5)$$

where $f_{\text{DBC}_{Ei}}$ represents the contribution from *i*th end-member. The fraction of ΔDBC to the total DBC_{BPCA} was noted as $f_{\Delta\text{DBC}}$.

Statistical analysis

Pearson regressions were performed to identify the linear change of various molecular parameters (oxygen-to-carbon ratio, molecular weight, DBE, modified aromaticity index, etc.) along the salinity gradient. The *t*-test was performed to analysis the differences in molecular composition among different groups of samples. Principle coordinate analysis (PCoA) based on the DBC_{FT} of all samples was performed to analyze the main molecular difference among different samples. All analyses were performed in the R language platform (RCoreTeam 2022).

Results

Temperature, salinity, and water masses

During our sampling, the water temperature ranged from 7.86°C to 18.02°C. It demonstrated a decreasing trend toward the north and at deeper depths in both the P and C sections (see Supporting Information Fig. S2). The salinity ranged from 28.25 to 34.58 across all samples. The T-S diagram illustrated that the P5 station had the highest salinity and temperature, suggesting the influence of the Taiwan Warm Current and Kuroshio Current (Chen 2009). Conversely, the surface layer of the P1 station in the Changjiang Estuarine region exhibited the lowest salinity, which is characteristic of the Changjiang Dilution Water (Supporting Information Fig. S2). Furthermore, the deep layers of the C5 and C6 stations had temperatures below 10°C, which is typical for the Yellow Sea Cold Water during the spring season (Chen 2009).

Distribution of DOC and DBC_{BPCA} in coastal seas

The concentration of DOC ranged from 44 to 112 μmol C L⁻¹, with the highest value at the surface layer of the P1 station and the lowest at the bottom layer of the P5 station (Table 1; Bao et al. 2023a). The concentration of DBC_{BPCA} ranged from 0.70 to 1.9 μmol C L⁻¹ and 0.97 to 1.7 μmol C L⁻¹ in the East China Sea and South Yellow Sea,

respectively (Fig. 2). Generally, DBC_{BPCA} concentrations were higher in surface waters and decreased with increasing water depth at most stations (Bao et al. 2023a). When comparing samples with similar salinity in the East China Sea, samples collected in the South Yellow Sea exhibited higher DBC_{BPCA} concentrations (Fig. 2).

The DBC_{BPCA}/DOC ratio was 1.1–2.8%, with a mean value of $1.9 \pm 0.4\%$ ($n = 37$, Table 1). The lowest and highest values were observed at the deep layer of P5 and the middle layer of C3, respectively (Bao et al. 2023a). The ratio of B6/B5 was 0.24–0.30 in all the samples, which showed no clear trend with salinity ($p > 0.05$) or downward water column (Table 1).

Molecular composition of DBC_{FT} in seawater samples and comparison with other aquatic samples

A total of 129 DBC_{FT} formulae were found in all the samples. The number of DBC_{FT} formulae in each sample ranged from 15 to 119, with an average of 90 ± 20 (Table 1). The intensity of DBC_{FT} accounted for 0.11% - 0.77% of the total intensity of each sample, which was significantly correlated with DBC_{BPCA} for all the samples ($R^2 = 0.44$, $p < 0.01$, $n = 37$; Table 1; Bao et al. 2023a). The intensity of DBC_{FT} provides information about the relative contribution of DBC_{FT} to total (SPE-)DOC, and due to the similar matrix, the percentage contribution can be directly compared among different samples.

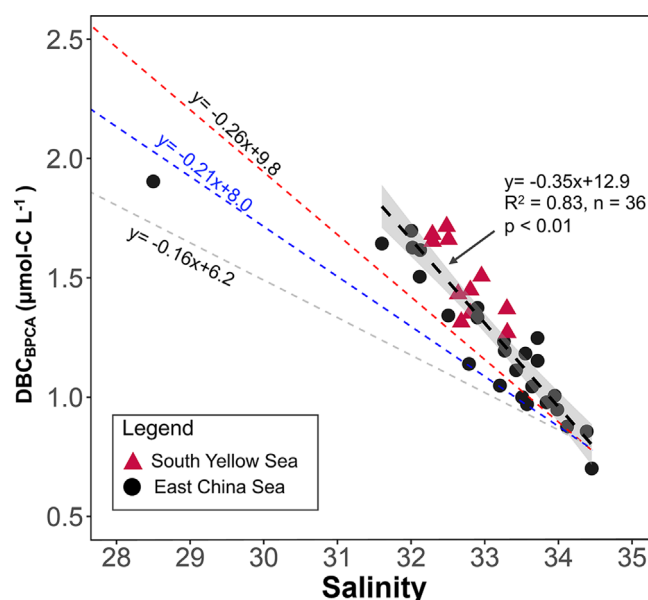


Fig. 2. The correlation between DBC_{BPCA} and salinity. Black dots and red triangles denote samples collected in the ECS and SYS, respectively. The correlation was performed by excluding the lowest salinity sample to avoid the influence from this single point. The DBC_{BPCA} for freshwater end-member was calculated based on the DBC concentration from Changjiang and Huanghe (Wang et al. 2016; Wang 2018). The red, blue, and gray dashed lines represent upper-, mean-, and lower- limit of the conservative mixing between riverine and offshore end-members.

Table 1. The minimum (Min), maximum (Max), mean, and standard deviation (SD) of the DBC_{BPCA} and DBC_{FT} parameters.

	<i>n</i>	Range (Min–Max)	Mean ± SD	Correlation coefficient with salinity
DOC	37	44–112	70 ± 15	–0.68**
DBC_{BPCA}				
DBC ($\mu\text{mol C L}^{-1}$)	37	0.70–1.9	1.3 ± 0.29	–0.83**
DBC_{BPCA}/DOC	37	0.011–0.028	0.019 ± 0.004	0.22
B6/B5	37	0.24–0.30	0.28 ± 0.01	0.14
DBC_{FT}				
Intensity (%)		0.11–0.77	0.47 ± 0.12	–0.68**
Formulae number	37	15–119	90 ± 20	–0.37*
H/C_wa	37	0.68–0.70	0.69 ± 0.005	0.06
O/C_wa	37	0.19–0.27	0.24 ± 0.02	–0.69**
N_wa	37	0.26–1.01	0.57 ± 0.15	0.14
S_wa	37	0–0.49	0.22 ± 0.11	0.01
DBE_wa	37	11–15	12 ± 1	0.56**
MW_wa	37	246–321	269 ± 17	0.57**
Almod_wa	37	0.69–0.70	0.70 ± 0.003	–0.54**
NOSC_wa	37	–0.25 – 0.01	–0.06 ± 0.05	–0.64**
CHO%	37	35–58	40 ± 5	–0.03
CHON%	37	22–49	40 ± 6	0.07
CHOS%	37	0–40	20 ± 8	–0.03

The suffix “wa” represents the intensity weighted average.

Al_{mod} , modified aromaticity index; DBE, double bond equivalent; MW, molecular weight; NOSC, normal oxidation state of carbon; S, sulfur content; N, nitrogen content; H/C, hydrogen to oxygen; O/C, oxygen to carbon ratio.

*Indicate significant level of $p < 0.05$;

**Indicate significant level of $p < 0.01$.

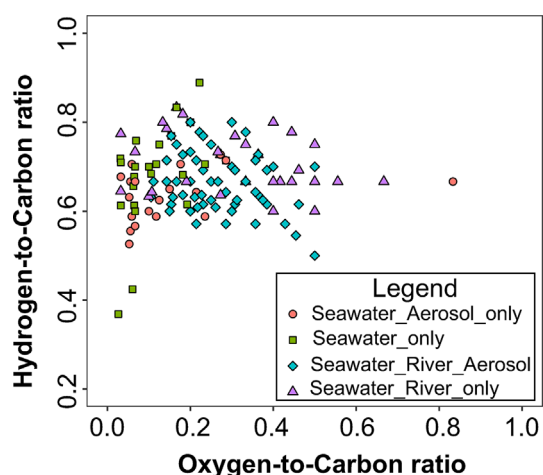


Fig. 3. Distribution of DBC formulae in different samples. van Krevelen diagram showing the oxygen-to-carbon- and hydrogen-to-carbon ratios of seawater DBC_{FT} also identified in aerosol and/or river samples. Seawater_Aerosol_only: present in both seawater and aerosol, but not in the river; Seawater_River_only: present in both seawater and river, but not in the aerosol; Seawater_River_Aerosol: present in seawater, river and aerosol; Seawater_only: only present in seawater samples.

However, DBC_{FT} does not allow quantification due to the lack of standards and the variable ionization efficiency of individual compounds that also depend on the sample matrix.

Molecular formulae containing only C, H, and O were defined as CHO formulae, C, H, O, and N as CHON formulae, and so forth. Among the 129 DBC_{FT} formulae, the majority belonged to the CHON category ($n = 52$), followed by CHO ($n = 43$) and CHOS ($n = 25$). Only three formulae were classified as CHONS and CHOP. The mean (\pm SD) fraction of CHO, CHON, and CHOS in each sample were $40 \pm 4.6\%$, $40 \pm 6.1\%$, and $20 \pm 8.4\%$, respectively (Table 1).

The oxygen-to-carbon ratio and hydrogen-to-carbon ratio ranges of DBC_{FT} were primarily distributed between 0.03 and 0.83 and between 0.36 and 0.89, respectively (Fig. 3). The intensity normalized heteroatom content S_{wa} and N_{wa} were 0–0.5 and 0.3–1.0 with a mean \pm SD value of 0.22 ± 0.11 and 0.57 ± 0.15 and were found to have no correlation with salinity (Table 1). Furthermore, the intensity normalized values of modified aromaticity index, molecular weight, the NOSC and DBE of DBC_{FT} were 0.69–0.70, 246–321, –0.25–0.01, and 11–15, respectively (Table 1). All of these parameters showed a significant correlation with salinity (Table 1).

Out of the total 129 formulae, 87 were detected in river water samples, accounting for 40–78% of the overall DBC_{FT} intensity in seawater. Similarly, 75 formulae were found in aerosols, representing 30–60% of the total DBC_{FT} intensity in seawater (Fig. 3; Bao et al. 2023a). Specifically, 56 formulae were present in both river water and aerosol samples (Seawater_River_Aerosol), while 31 formulae were exclusively

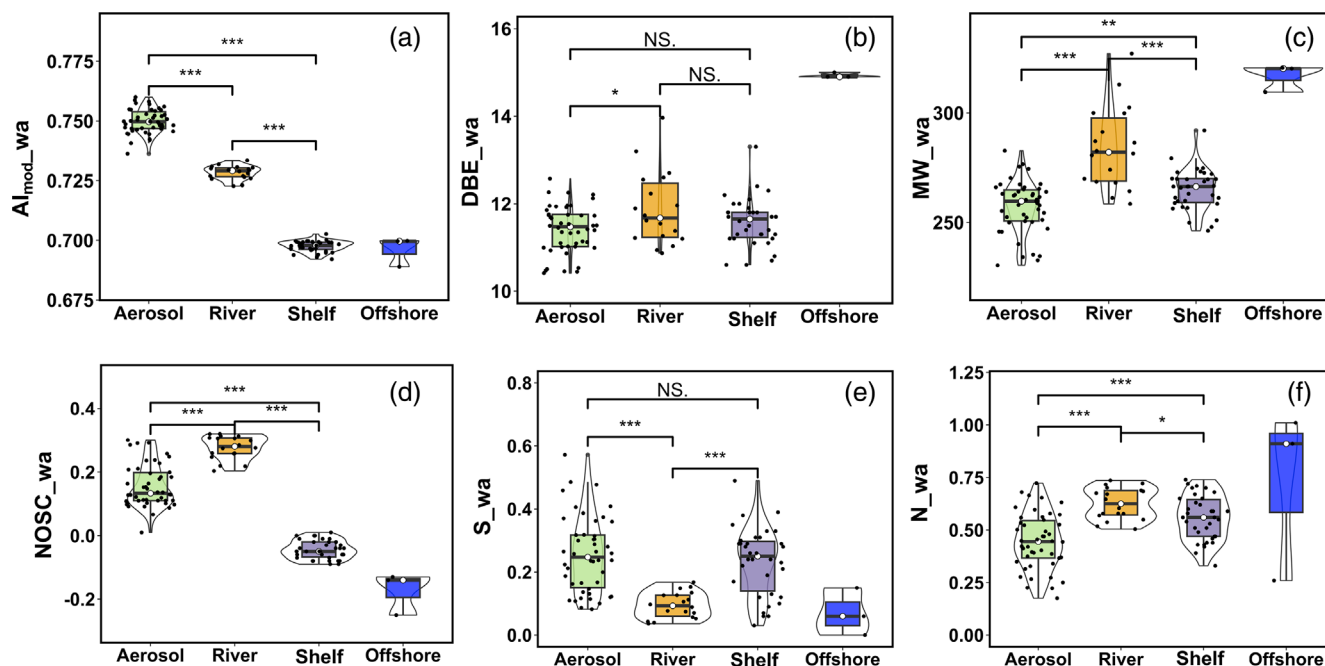


Fig. 4. The distribution and comparison of the molecular composition of DBC_{FT} among sample groups. The offshore group includes the P5 station, while shelf includes all other seawater samples. NS., non-significant; *, **, *** indicate significance level of $p < 0.05$, $p < 0.01$, and $p < 0.001$ for the t -test analysis, respectively. The Offshore group was excluded from the analysis due to the limited number of samples ($n = 3$). The parameters shown were all intensity normalized. (a) Al_{mod_wa}: modified aromaticity index; (b) DBE_{wa}: double bond equivalent; (c) MW_{wa}: molecular weight; (d) NOSC_{wa}: nominal oxidation state of carbon; (e) S_{wa}: sulfur content; (f) N_{wa}: nitrogen content. The DBC_{FT} data for aerosols are from previous studies (Bao et al. 2017, 2018).

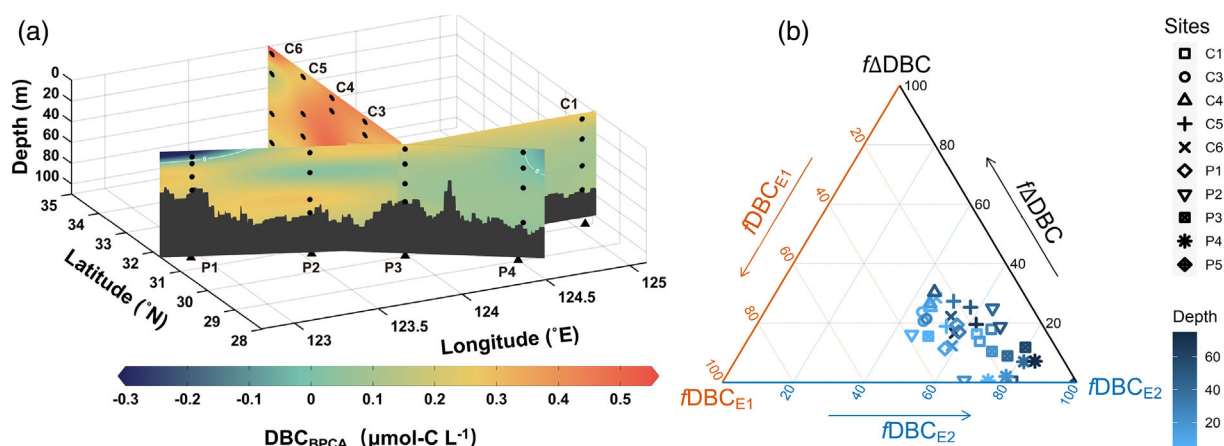


Fig. 5. The end-member model results. (a) The distribution of ΔDBC ($\mu\text{mol C L}^{-1}$) in the sampling regions. The white lines indicate $0 \mu\text{mol C L}^{-1}$, which means no input or removal. (b) The distribution of contribution (%) of freshwater ($f\text{DBC}_{E1}$), offshore ($f\text{DBC}_{E2}$), and other sources ($f\Delta\text{DBC}$) to the total DBC_{BPCA} in each sample.

found in river water and 19 formulae were exclusively found in aerosols (Fig. 3). At the offshore P5 station, $\sim 40\%$ of the DBC_{FT} , in terms of both intensity and number of formulae, could not be identified in either river water or aerosols (Supporting Information Table S1).

The DBC_{FT} found in seawater exhibited lower intensity normalized indices of modified aromaticity index, and NOSC compared to both riverine and aerosol samples (Fig. 4). However, in terms of intensity normalized N-content, the DBC_{FT} in seawater was similar to riverine samples but higher than

aerosol samples. By contrast, the intensity normalized sulfur content in seawater was similar to aerosol samples but higher than in riverine samples (Fig. 4).

End-member mixing model results

The value for the freshwater end-member of DBC_{BPCA} was determined as the discharge-weighted value of major rivers that contribute to the study area, which was estimated to be $8.0 \pm 1.8 \mu\text{mol C L}^{-1}$. This value was calculated using monthly data from the Changjiang and Huanghe rivers, taking into

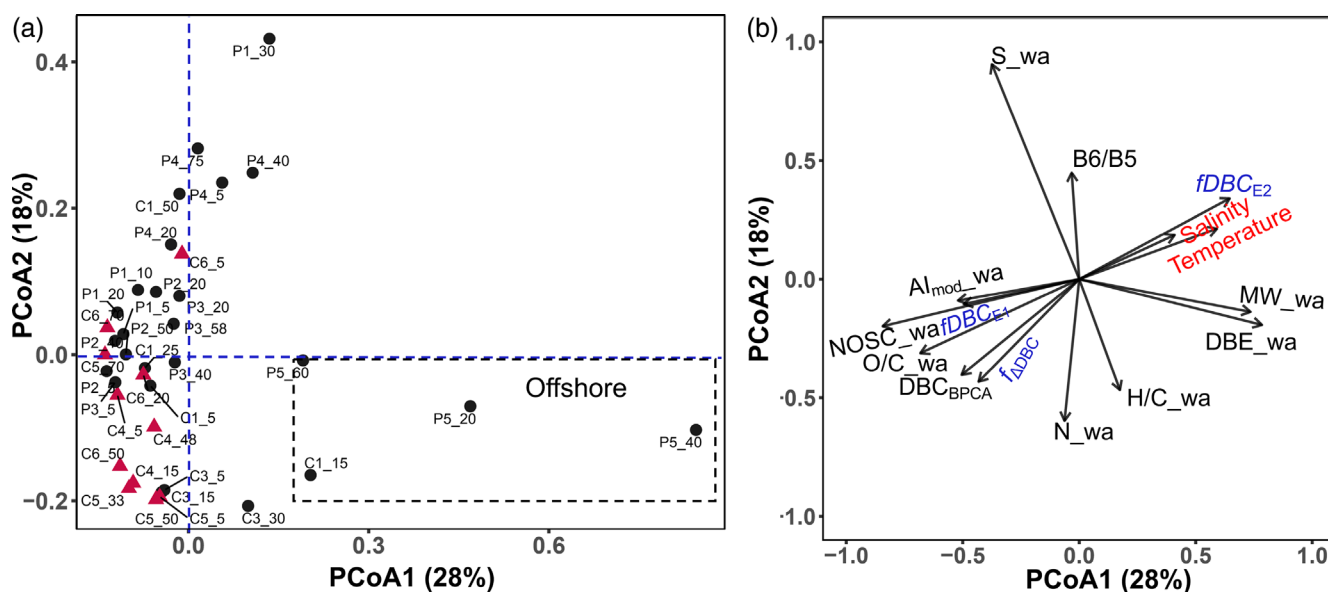


Fig. 6. PCoA analysis based on the molecular composition of DBC_{FT} . (a) the PCoA scores of each sample with red triangles representing the South Yellow Sea and black circles representing the East China Sea samples. Offshore samples are highlighted in the box; (b) the Pearson's correlation coefficient of different parameters with the PCoA 1 and PCoA2 scores of each sample, with molecular indices in black, environmental factors displayed in red and contribution from each source in blue. The suffix wa represents intensity weighted value. Al_{mod} , modified aromaticity index; DBE, double bond equivalent; MW, molecular weight; NOSC, normal oxidation state of carbon; S, sulfur content; N, nitrogen content; H/C, hydrogen-to-carbon ratio; O/C, oxygen-to-carbon ratio.

account the potential impact of other rivers (refer to Supporting Information Data S1 for detailed calculations) (Wang et al. 2016; Wang 2018). According to the T-S diagram described in section 2.1, the P5 station exhibited characteristics typical of the Taiwan Warm Current and Kuroshio Current. Since the surface and bottom layers of P5 were potentially contaminated, the average salinity and DBC_{BPCA} of the three intermediate layers at P5 were considered as the end-member values for S_{E2} and DBC_{E2} , respectively, yielding values of 34.32 ± 0.2 and 0.81 ± 0.037 , respectively.

With the exception of the surface layer of P1, the ΔDBC increased along transect C from $0.003 \pm 0.11 \mu\text{mol CL}^{-1}$ at the bottom of C1 station to $0.52 \pm 0.14 \mu\text{mol CL}^{-1}$ at the bottom of C4 station (Fig. 5a; Bao et al. 2023a), and the $fDBC_{E1}$ and $f\Delta DBC$ was 6–37% and 0–30%, respectively (Fig. 5b). Deviation “±” is assessed from the error propagation considering the variation in end-member values, which included freshwater DBC_{BPCA} , offshore DBC_{BPCA} , and offshore salinity. Additionally, the ΔDBC of the surface layer of P1 indicated a removal trend of $-0.18 \pm 0.32 \mu\text{mol CL}^{-1}$ (Bao et al. 2023a).

Principal coordinate analysis

The first two components of the PCoA accounted for 27.9% and 18.0% of the variation of DBC_{FT} , respectively

(Fig. 6). PCoA1, the first component, primarily differentiated the offshore station P5 from the other samples and showed a significant positive relationship with the intensity normalized molecular weight and DBE, while displaying a significant negative relationship with the NOSC. PCoA2, the second component, mainly distinguished between the samples from the East China Sea and South Yellow Sea, exhibiting a significant positive correlation with sulfur content ($r = 0.90$, $n = 37$, $p < 0.01$) and a negative relationship with nitrogen content ($r = -0.6$, $n = 37$, $p < 0.01$).

Discussion

Variation in DBC_{BPCA} concentration in coastal seas: Sources and influencing processes

Sources of DBC_{BPCA}

The concentrations of DBC_{BPCA} in the East China Sea and the South Yellow Sea ($0.70\text{--}1.9 \mu\text{mol CL}^{-1}$) fall within the reported range for coastal seas with similar salinity levels, such as the Canada Basin and the South China Sea (Fang et al. 2017, 2021c; Table 2), and are higher than reports for the open ocean (see Table 2 and references therein). The lowest DBC_{BPCA} concentrations observed at station P5 ($0.70\text{--}0.88 \mu\text{mol L}^{-1}$) were similar to DBC levels measured in the

Table 2. Comparison of DBC_{BPCA} concentration in global coastal and open oceans.

Region	Salinity range	DBC_{BPCA} ($\mu\text{mol CL}^{-1}$)	References
Coastal Sea			
East China Sea	28.5–34.5	0.6–1.9	This study
Chukchi Sea	29–32	0.7–1.0	Nakane et al. 2017
Bering Sea	30.5–33	0.3–0.9	Nakane et al. 2017
Bering Sea	28.5–34.5	0.7–3.8	Fang et al. 2021c
Chukchi Sea	26–32.5	1.0–1.5	Fang et al. 2021c
Canada Basin	28–35	0.8–1.8	Fang et al. 2021c
Bohai Bay and Laizhou Bay	22–31	1.8–5.6	Fang et al. 2021b
South China Sea	32–34	0.6–1.6	Fang et al. 2017
Bohai Sea	25–32	0.2–5.3	Fang et al. 2021a
Sargasso Sea	/	1.2/1.8	Coppola and Druffel 2016
Open Ocean			
Subarctic North Pacific	32.5–34	0.4–0.7	Nakane et al. 2017; Mori et al. 2021
Subtropical North Pacific	34–35	0.6–0.7	Nakane et al. 2017
Pacific Ocean (50 N–40°S)	/	0.2–0.5	Yamashita et al. 2022
Prydz Bay shelf	32.6–34.7	0.4–1.5	Fang et al. 2018
Northeast Pacific	/	1.4	Coppola and Druffel 2016
Beaufort Sea	/	1.7/2.6	Coppola and Druffel 2016
Northeast Atlantic	/	1.5	Coppola and Druffel 2016
South Atlantic	/	2.4	Coppola and Druffel 2016
Coastal Arctic	/	1.5	Coppola and Druffel 2016
Pacific	/	0.6	Wagner et al. 2019a; Wagner et al. 2019b
Atlantic	/	0.7–0.8	Wagner et al. 2019a; Wagner et al. 2019b
Antarctic	/	0.6–0.8	Dittmar and Paeng 2009

/, data not available.

Pacific Ocean ($0.4\text{--}0.7\ \mu\text{mol L}^{-1}$; Nakane et al. 2017) (Table 2), which is consistent with the origin of the water mass (the Pacific Ocean), and also support the selection of this station as offshore source end-member.

DBC primarily originates from the incomplete combustion of biomass and fossil fuel on land and is transported to the ocean through various pathways, including riverine discharge, atmospheric deposition, and tidal pumping from coastal wetlands (Dittmar et al. 2012; Jaffe et al. 2013; Bao et al. 2017; Jones et al. 2020). While fresh groundwater could potentially be a source of DBC, it has been reported to be relatively depleted in condensed aromatics (McDonough et al. 2022). Excluding the surface sample of the P1 station (which had the lowest salinity), the concentration of DBC_{BPCA} in all other samples showed a significant negative correlation with salinity (Fig. 2), indicating that DBC is primarily associated with freshwater discharge, consistent with findings in the Bering Sea, the Canada Basin, the Bohai Sea, and the South China Sea (Fang et al. 2017, 2021a, 2021c). The concentration of DBC_{BPCA} in coastal rainwater (mean: $0.56\text{--}1\ \mu\text{mol C L}^{-1}$) is typically lower than that in seawater (Bao et al. 2022; Wagner et al. 2019b). Therefore, riverine discharge plays a crucial role in delivering DBC to the South Yellow Sea and East China Sea shelf, which is also consistent with other river-dominated ocean margins, such as the Bohai, Yellow Sea, and Bering Sea (Fang et al. 2021a, 2021b, 2021c). The correlation coefficient between DBC_{BPCA} and DOC in the coastal samples ($R^2 = 0.26$) further indicates that they are influenced by different primary sources/processes. Previous studies suggest that DOC in the East China Sea is primarily related to phytoplankton production and microbial transformation (Yu et al. 2016; Kim et al. 2020). Thus, the decoupling between the two parameters supports a primarily terrestrial source of DBC.

The surface layer of P1 exhibited the highest concentration of DBC_{BPCA} , which was associated with the lowest salinity and indicated input from the river. The much lower salinity at the surface layer (28.25) compared to deeper layers of P1 (> 32.5 , Bao et al. 2023a) reflected the direct influence from the Changjiang. Extrapolating a conservative mixing line between the surface layer of P1 and the offshore end-member resulted in a freshwater end-member concentration of $\sim 7\ \mu\text{mol C L}^{-1}$ (Fig. 2). This value closely matched the DBC_{BPCA} concentration of the Changjiang in spring ($6\text{--}8\ \mu\text{mol C L}^{-1}$; Wang 2018), further supporting the direct influence from the Changjiang on the surface layer of P1.

In almost all other samples, DBC_{BPCA} concentrations were higher than what could be explained by the two-end-member mixing model (Fig. 5a). The main error was attributed to the variation in the end-member value of freshwater DBC_{BPCA} . However, even considering the propagated error from the variation of the end-member, the calculated DBC_{BPCA} concentrations still indicated an additional source of DBC in most samples (Bao et al. 2023a). The contribution from this additional input was comparable to that of riverine discharge in

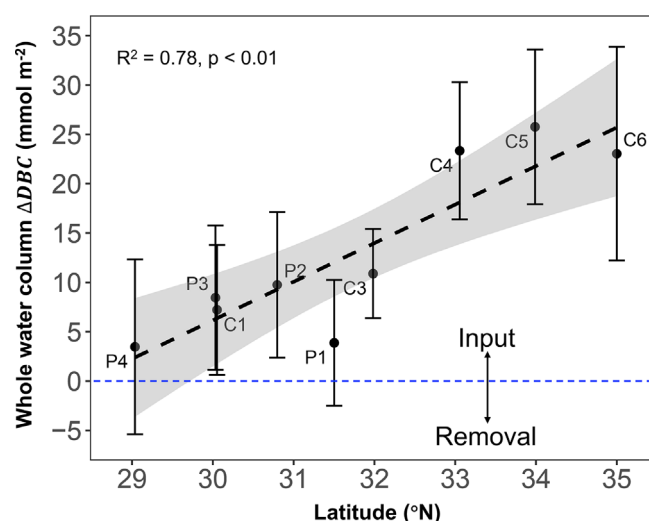


Fig. 7. The total ΔDBC integrated over the whole water column at each station. Error bars indicate the estimation error from the propagated error of ΔDBC . Positive and negative values indicate input and removal, respectively.

this region (Fig. 5b). Integrating over the entire water column (obtained from the mathematical area of ΔDBC with respect to depth by using OriginPro [2023]), the estimated addition of DBC_{BPCA} ranged from $3.5 \pm 8.9\ \text{mmol m}^{-2}$ (P4) to $26 \pm 7.8\ \text{mmol m}^{-2}$ (C5), and showed a significant positive correlation with latitude (Fig. 7). This addition amount should be treated as the net results between the removal and input, which further indicates additional sources played a more critical role than riverine discharge in this region.

Atmospheric deposition of DBC_{BPCA} is considered significant on both global and regional scales (Bao et al. 2017; Zhang et al. 2023; Zhao et al. 2023). A previous study has shown that dry deposition of DBC_{BPCA} in the study area accounted for $\sim 40\%$ of the quantitatively most relevant riverine input in spring, with a decreasing trend southward. The main sources of atmospheric DBC_{BPCA} during the study period were dust and haze (Bao et al. 2017). Ship emission could also be a potential source of BC in the ocean (Lack and Corbett 2012), which may contribute to the DBC pool after photo-oxidation/dissolution (Decesari et al. 2002; Zhang et al. 2023). The ratio of B6/B5 in most stations was within the range for riverine discharge (range: $0.26\text{--}0.31$; Bao et al. 2019) and aerosols (range: $0.15\text{--}0.39$; Bao et al. 2017), indicating the input from both sources.

We further constrained the atmospheric deposition flux to assess whether atmospheric deposition itself could sustain the increment of DBC_{BPCA} in the study region. By considering the reported values of dry and wet deposition of DOC and the $\text{DBC}_{\text{BPCA}}/\text{DOC}$ ratio in different areas, we estimated the total deposition of DBC_{BPCA} to be $0.34\ \text{mmol m}^{-2}\ \text{yr}^{-1}$ in the offshore and $2.3\ \text{mmol m}^{-2}\ \text{yr}^{-1}$ in the nearshore area (see Supporting Information Data S1 for calculation). These

estimates are comparable to the average atmospheric deposition of DBC_{BPCA} in the Bohai Sea ($\sim 1 \pm 0.5 \text{ mmol m}^{-2} \text{ yr}^{-1}$; Fang et al. 2018). However, it is important to note that our estimates may represent an upper limit for atmospheric deposition due to two reasons: (1) we used a calculation based on 365 d for dry deposition; (2) the wet deposition flux of DOC in the nearshore region was from a coastal island ($3.15 \text{ g m}^{-2} \text{ yr}^{-1}$; Xing et al. 2019), which may lead to overestimation since our sites were further away from the coast because atmospheric wet deposition typically decreases with increasing proximity to the land (Iavorivska et al. 2016).

The residence time of water, as determined by the Ra isotope, was reported to be 2–5 years, with a mean value of 4 years in the study region (Men and Liu 2014). Based on this information, we estimated that atmospheric deposition contributed 1.2 to $9.2 \text{ mmol C m}^{-2}$ of DBC_{BPCA} in the offshore and coastal regions, respectively, during the residence period. Despite the inherent uncertainties in these estimations, the significant discrepancy between the estimated increment of DBC and atmospheric deposition suggests that atmospheric deposition alone cannot account for the increase in DBC_{BPCA} , indicating the presence of other sources in the region.

The contribution from coastal wetlands, desorption from particles, and sediment porewaters are other potential sources. In the turbidity maximum zone in the Changjinag Estuary during the dry season, a substantial addition of chromophoric/colored DOM (as indicated by light absorbance at 355 nm, a_{355}) was observed (Guo et al. 2014), which was found to be highly significantly correlated with DBC_{BPCA} in Arctic rivers (Stubbins et al. 2015). This addition was suggested to be related to the resuspension of sediments, porewater, and contribution from the wetlands resulting from the tidal movement (Guo et al. 2014). Additionally, Liu et al. (2021) quantified that porewater exchange from coastal wetlands in the Changjiang coastal area contributed ~ 1.2 times the riverine discharge of DOC. Previous studies have also shown the enrichment of DBC_{BPCA} in porewater from wetlands and sandy beaches (Dittmar et al. 2012; Ding et al. 2014; Seidel et al. 2014). Therefore, it is reasonable to deduce that tidal pumping from coastal wetlands could be another significant source of DBC_{BPCA} , although it needs to be quantified. Furthermore, the BPCA was also identified in the petrogenic origins, such as crude oil (Hindersmann and Achten 2017) and petroleum (Goranov et al. 2021). Consequently, the discharge of ship fuel directly into the water may serve as an additional plausible source. Nevertheless, our results indicated that besides rivers and atmospheric deposition, there are other important sources in this region that should be quantified and included in the regional DBC_{BPCA} budgets in the future.

Processes affecting DBC_{BPCA}

The concentration of DBC_{BPCA} exhibited a variation of approximately threefold across the study area, which is consistent with the range observed in the South China Sea (Fang

et al. 2017) and Arctic coastal seas (Fang et al. 2021c). The significant correlation between DBC_{BPCA} and salinity suggests that the mixing of water masses plays a dominant role in regulating the variation in DBC_{BPCA} concentration.

The removal of DBC_{BPCA} from the water column is primarily attributed to photo-degradation and sorption by particles. Both processes have been found to preferentially remove condensed aromatics, leading to a lower B6/B5 ratio (Stubbins et al. 2012; Yamashita et al. 2022). Interestingly, our observations indicate a net input of DBC_{BPCA} , which contrasts with the significant removal observed in the Bering Sea and the Canada Basin (Fang et al. 2021c). We hypothesize that this discrepancy is due to the strong influence of regional inputs, which mask the removal process. It is important to note that photodegradation mainly occurs in the surface layer of the water column, as ultraviolet light attenuates quickly with depth (Huovinen et al. 2003). Consistent with the input trend, the B6/B5 ratio in the surface layer was not lower in most stations (Bao et al. 2023a), indicating the strong influence of other sources on the condensation degree of DBC_{BPCA} .

Molecular composition of DBC_{FT} : Sources and influencing factors

Sources indications from the molecular composition of DBC_{FT}

The molecular evidence provided by DBC_{FT} indicated the sources of DBC. The presence of $\sim 80\%$ of seawater DBC_{FT} (in terms of both the number of formulae and intensity) in the riverine and aerosol samples indicated them as primary sources of DBC_{FT} (Fig. 3). However, it is important to consider factors such as ionization efficiency and matrix effect (e.g., differences between seawater and aerosols) that can influence the detection of DBC_{FT} . The intensity of DBC_{FT} in seawater is relatively lower ($< 1\%$) compared to riverine (2.9–4.7%) and aerosol samples (1.3–10%), which may impact the identification of low-intensity compounds (Bao et al. 2017), and consequently affect its molecular characteristics. Therefore, due to the overlap of DBC_{FT} between seawater, aerosols, and rivers (Seawater_River_Aerosol formulae in Fig. 3), as well as differences in ionization efficiency, the relative contribution of these sources could not be quantified based on molecular composition alone. Furthermore, the identification of seawater_river DBC_{FT} is potentially to be biased because of the variation in the end member. It was found that the molecular composition of DBC_{FT} , especially the nitrogen content, was affected by agriculture coverage (Wagner et al. 2015). Although covering a whole hydrograph, differences in agricultural coverage between the Chanjiang (the primary freshwater source in the study area) and the North Jiulong River (used for comparison) may bias the identification of river-derived formulae, especially those nitrogen-containing compounds (Bao et al. 2023b). Other factors to consider include the possibility that the same formulae may represent different compounds with diverse structures and that some formulae found in rivers

or aerosols may also come from unidentified sources. Nevertheless, the molecular composition of DBC_{FT} was generally in line with the information from DBC_{BPCA} . Approximately 20% of the formulae were specific to seawater (seawater_only formulae; Fig. 3), which could be explained by limited riverine samples, unidentified sources such as tidal wetlands, or deoxygenation/decarboxylation processes during photodegradation (Zhao et al. 2023).

Molecular-level differences and influencing factors

Like the DBC_{BPCA} , the molecular parameters (molecular weight, NOSC, and DBE) of DBC_{FT} showed significant correlations with salinity (Table 1). These correlations indicate the impact of mixing processes on the molecular composition of DBC_{FT} . Most of the DBC_{FT} parameters fell within the range observed in river water/aerosol and offshore P5 station samples, further supporting the idea of mixing among these sources (Fig. 4). The intensity normalized modified aromaticity index varied slightly (0.69–0.70), but its range and correlation with salinity were consistent with the mixing process. However, it is important to note that the R^2 values between the DBC_{FT} indices and salinity were all $< 50\%$ in our study (Table 1). This suggests that there are other significant factors at play, including variations in end-member values, input from unidentified sources, and/or removal processes.

PCoA based on DBC_{FT} composition revealed distinct molecular differences between offshore and coastal samples (PCoA 1) and between the East China Sea and South Yellow Sea samples (PCoA 2) (Fig. 6a). DBC_{FT} in the offshore P5 station exhibited higher molecular weight, lower modified aromaticity, and lower nominal oxidation state of carbon compared to other coastal seawater samples. Both photo-degradation and sorption by particles may have an impact on the DBC_{FT} in the open ocean. While sorption has been suggested as the primary process for removing DBC in the open ocean (Yamashita et al. 2022), its influence on DBC_{FT} is still unclear. A previous study found that sorption would preferentially adsorb compounds with rich oxygen content from biochar leachate, which would leave compounds with lower nominal oxidation of carbon (Luo et al. 2019). Photodegradation has the potential to effectively eliminate nearly all DBC_{FT} (Stubbins et al. 2010). However, this process may generate new DBC_{FT} compounds with higher molecular weight (Stubbins et al. 2010), which could potentially account for the observed increase in molecular weight of DBC_{FT} at P5.

PCoA 2 mainly distinguished East China Sea samples from South Yellow Sea samples, and the main distinguishing factors were the content of sulfur and nitrogen (Fig. 6b). A significant negative correlation was observed between PCoA 2 and $\Delta DBC/DBC_{BPCA}$ ($f\Delta DBC$) ($R^2 = 0.19$, $n = 37$, $p < 0.01$). This suggests that the net addition of DBC, which represents the balance between input and removal, may have an influence on the observed differences. The variability in the riverine end-member could also contribute to the observed variations.

For instance, as discussed in section 3.2.1, the nitrogen content was found to be associated with the extent of agricultural activities in the watershed (Wagner et al. 2015), which may differ between the freshwater discharged into the East China Sea and the Yellow Sea. Furthermore, during the sorption of DOM, fractionation also occurred in terms of heteroatom, leading to a preferential removal of dissolved organic sulfur over dissolved organic nitrogen (Luo et al. 2019). However, due to the complexity of the processes involved and the limited understanding of the molecular composition of DBC from regional sources, it is challenging to pinpoint the specific factor responsible for the observed differences. To gain a better understanding of the sources and processing of DBC in the ocean, further investigations focusing on the molecular composition of potential sources and the effects of different processes on DBC are warranted.

Conclusions and implications

A comprehensive understanding of the origins and cycling of DBC in the coastal ocean is crucial for accurately predicting potential future changes in this long-lasting carbon pool. By combining BPCA and FT-ICR-MS methods, the sources and processes that control DBC in the coastal sea were identified. Our findings in the coastal seas have unveiled significant inverse relationships between DBC_{BPCA} and salinity, as well as between molecular indices of DBC_{FT} (such as NOSC and DBE) and salinity. These findings indicate that mixing processes predominantly regulate the concentration and compositional changes of DBC.

Using a two-end-member mixing model, we further estimated that, in addition to riverine discharge, there are strong additional sources in the East China Sea and South Yellow Sea that contribute to DBC to a similar extent. Moreover, our estimates indicate that atmospheric deposition alone cannot sustain the increase in DBC in the coastal region. Therefore, there are unidentified sources that require further quantification in future studies. The molecular composition of DBC further supported the input from riverine discharge and atmospheric deposition, as $\sim 70\%$ and $\sim 60\%$ of seawater DBC_{FT} could be found in river water and aerosols, respectively. However, $\sim 20\%$ of DBC_{FT} remains unidentified, which could be attributed to either unknown sources or modifications through various processes.

The sources of DBC in the ocean are still debatable, primarily due to significant differences in the stable isotope composition of DBC between riverine and oceanic samples (Wagner et al. 2019a). Our study indicates that non-riverine sources play an almost equal role as rivers in delivering DBC to the coastal sea on a regional scale. This highlights the need to identify and quantify new DBC sources on both regional and global scales (Coppola et al. 2022). However, due to the overlapping molecular composition among different sources, it is challenging to track the origins of DBC using single tools.

Therefore, future studies should simultaneously measure the concentration, molecular composition, and isotopic composition of DBC to explore the inputs from other sources and understand how different processes may modify the molecular composition of DBC.

Data availability statement

All the data used in this study were provided in two datasets. Dataset 01 includes the DBC_{BPCA}, indices of DBC_{FT}, and the results of end-member mixing model; Dataset 02 includes the molecular formulae and relative intensity of DBC_{FT} for each sample. Both of the datasets were deposited in Figshare under the license of Creative Commons Attribution 4.0 (CC BY 4.0). The data can be accessed through the following link: <https://doi.org/10.6084/m9.figshare.23715279.v1> and was cited in the main text as Bao et al. (2023a).

References

- Bao, H. Y., J. Niggemann, L. Luo, T. Dittmar, and S. J. Kao. 2017. Aerosols as a source of dissolved black carbon to the ocean. *Nat. Commun.* **8**. doi:10.1038/s41467-41017-00437-41463
- Bao, H., J. Niggemann, L. Luo, T. Dittmar, and S.-J. Kao. 2018. Molecular composition and origin of water-soluble organic matter in marine aerosols in the Pacific off China. *Atmos. Environ.* **191**: 27–35.
- Bao, H., J. Niggemann, D. Huang, T. Dittmar, and S. J. Kao. 2019. Different responses of dissolved black carbon and dissolved lignin to seasonal hydrological changes and an extreme rain event. *J. Geophys. Res. Biogeo.* **124**: 479–493.
- Bao, H., and others. 2022. Multiproxy probing of anthropogenic influences on the different components of dissolved organic matter in coastal rainwater. *Sci. Total Environ.* **824**. doi:10.1016/j.scitotenv.2022.153846
- Bao, H., and others. 2023a. Supporting data for “deciphering sources and processing of dissolved black carbon (DBC) in coastal seas”. figshare. Dataset. doi:10.6084/m9.figshare.23715279.v1
- Bao, H., and others. 2023b. Global riverine export of dissolved lignin constrained by hydrology, geomorphology, and land-cover. *Global Biogeochem. Cy.* **37**: e2022GB007607.
- Bostick, K. W., A. R. Zimmerman, A. I. Goranov, S. Mitra, P. G. Hatcher, and A. S. Wozniak. 2021. Biolability of fresh and photodegraded pyrogenic dissolved organic matter from laboratory-prepared chars. *J. Geophys. Res. Biogeosci.* **126**. doi:10.1029/2020JG005981
- Chen, C.-T. A. 2009. Chemical and physical fronts in the Bohai, yellow and East China seas. *J. Mar. Syst.* **78**: 394–410.
- Chen, Y., K. Sun, Z. Wang, E. Zhang, Y. Yang, and B. Xing. 2022. Analytical methods, molecular structures and biogeochemical behaviors of dissolved black carbon. *Carbon Res.* **1**: 23.
- Coppola, A. I., L. A. Ziolkowski, C. A. Masiello, and E. R. M. Druffel. 2014. Aged black carbon in marine sediments and sinking particles. *Geophys. Res. Lett.* **41**: 2427–2433.
- Coppola, A. I., and E. R. M. Druffel. 2016. Cycling of black carbon in the ocean. *Geophys. Res. Lett.* **43**: 4477–4482.
- Coppola, A. I., and others. 2019. Marked isotopic variability within and between the Amazon River and marine dissolved black carbon pools. *Nat. Commun.* **10**: 4018.
- Coppola, A. I., and others. 2022. The black carbon cycle and its role in the earth system. *Nat. Rev. Earth Environ.* **3**: 516–532.
- Decesari, S., and others. 2002. Water soluble organic compounds formed by oxidation of soot. *Atmos. Environ.* **36**: 1827–1832.
- Ding, Y., K. M. Cawley, C. N. da Cunha, and R. Jaffé. 2014. Environmental dynamics of dissolved black carbon in wetlands. *Biogeochemistry* **119**: 259–273.
- Dittmar, T., B. Koch, N. Hertkorn, and G. Kattner. 2008. A simple and efficient method for the solid-phase extraction of dissolved organic matter (SPE-DOM) from seawater. *Limnol Oceanogr Meth* **6**: 230–235.
- Dittmar, T., and J. Paeng. 2009. A heat-induced molecular signature in marine dissolved organic matter. *Nat. Geosci.* **2**: 175–179.
- Dittmar, T., J. Paeng, T. M. Gihring, I. G. N. A. Suryaputra, and M. Huettel. 2012. Discharge of dissolved black carbon from a fire-affected intertidal system. *Limnol. Oceanogr.* **57**: 1171–1181.
- Fang, Z., W. Yang, M. Chen, M. Zheng, and W. Hu. 2016. Abundance and sinking of particulate black carbon in the western Arctic and subarctic oceans. *Sci. Rep.* **6**: 29959.
- Fang, Z., W. Yang, M. Chen, and H. Ma. 2017. Source and fate of dissolved black carbon in the Western South China Sea during the southwest monsoon prevailing season. *J. Geophys. Res. Biogeo.* **122**: 2817–2830.
- Fang, Y., and others. 2018. Cycling and budgets of organic and black carbon in coastal Bohai Sea, China: Impacts of natural and anthropogenic perturbations. *Global Biogeochem. Cy.* **32**: 971–986.
- Fang, Y., and others. 2021a. Particulate and dissolved black carbon in coastal China seas: Spatiotemporal variations, dynamics, and potential implications. *Environ. Sci. Technol.* **55**: 788–796.
- Fang, Y., Huang, G., Chen, Y., Hu, L., Lin, J., and Lin, T. 2021b. Particulate and Dissolved Black Carbon in Bohai and Laizhou Bays, China: Distributions, Sources, and Contrasts Under Two Distinct Fluvial Hydrological Regimes. *Front. Earth Sci.* **9**: 697728.
- Fang, Z., and others. 2021c. Spatial characteristics and removal of dissolved black carbon in the western Arctic Ocean and Bering Sea. *Geochim. Cosmochim. Acta* **304**: 178–190.
- Geng, X., and others. 2021. Year-round measurements of dissolved black carbon in coastal Southeast Asia aerosols: Rethinking its atmospheric deposition in the ocean.

- J. Geophys. Res. Atmospheres. **126**. doi:10.1029/2021jd034590
- Goranov, A. I., M. F. Schaller, J. A. Long, D. C. Podgorski, and S. Wagner. 2021. Characterization of Asphaltenes and petroleum using Benzenepolycarboxylic acids (BPCAs) and compound-specific stable carbon isotopes. *Energy Fuel* **35**: 18135–18145.
- Guo, W., and others. 2014. Runoff-mediated seasonal oscillation in the dynamics of dissolved organic matter in different branches of a large bifurcated estuary—the Changjiang estuary. *J. Geophys. Res. Biogeo.* **119**: 776–793.
- Hindersmann, B., and C. Achten. 2017. Accelerated benzene polycarboxylic acid analysis by liquid chromatography–time-of-flight–mass spectrometry for the determination of petrogenic and pyrogenic carbon. *J. Chromatogr. A* **1510**: 57–65.
- Huovinen, P. S., H. Penttila, and M. R. Soimasuo. 2003. Spectral attenuation of solar ultraviolet radiation in humic lakes in Central Finland. *Chemosphere* **51**: 205–214.
- Hwang, J. H., S. P. Van, B.-J. Choi, Y. S. Chang, and Y. H. Kim. 2014. The physical processes in the Yellow Sea. *Ocean & Coastal Management* **102**: 449–457.
- Iavorivska, L., E. W. Boyer, and D. R. DeWalle. 2016. Atmospheric deposition of organic carbon via precipitation. *Atmos. Environ.* **146**: 153–163.
- Jaffe, R., and others. 2013. Global charcoal mobilization from soils via dissolution and riverine transport to the oceans. *Science* **340**: 345–347.
- Jones, M. W., and others. 2019. Environmental controls on the riverine export of dissolved black carbon. *Global Biogeochem. Cy.* **33**: 849–874.
- Jones, M. W., and others. 2020. Fires prime terrestrial organic carbon for riverine export to the global oceans. *Nat. Commun.* **11**: 2791.
- Kim, J., T. H. Kim, S. R. Park, H. J. Lee, and J. K. Kim. 2020. Factors controlling the distributions of dissolved organic matter in the East China Sea during summer. *Sci. Rep.* **10**: 11854.
- Koch, B. P., and T. Dittmar. 2006. From mass to structure: An aromaticity index for high-resolution mass data of natural organic matter. *Rapid Commun. Mass Spectrom.* **20**: 926–932.
- Koch, B. P., T. Dittmar, M. Witt, and G. Kattner. 2007. Fundamentals of molecular formula assignment to ultrahigh resolution mass data of natural organic matter. *Anal. Chem.* **79**: 1758–1763.
- Koch, B. P., and T. Dittmar. 2016. From mass to structure: An aromaticity index for high-resolution mass data of natural organic matter. *Rapid Commun. Mass Spectrom.* **30**: 250.
- Kuo, L. J., P. Louchouart, and B. E. Herbert. 2011. Influence of combustion conditions on yields of solvent-extractable anhydrosugars and lignin phenols in chars: Implications for characterizations of biomass combustion residues. *Chemosphere* **85**: 797–805.
- Lack, D. A., and J. J. Corbett. 2012. Black carbon from ships: A review of the effects of ship speed, fuel quality and exhaust gas scrubbing. *Atmos Chem Phys* **12**: 3985–4000.
- Lian, E., and others. 2022. Unraveling the synoptic-scale penetration of the Yellow Sea coastal water into the Changjiang River estuary. *J. Geophys. Res. Oceans* **127**: e2022JC018773.
- Liu, J., X. Yu, X. Chen, J. Du, and F. Zhang. 2021. Utility of radium quartet for evaluating porewater-derived carbon to a saltmarsh nearshore water: Implications for blue carbon export. *Sci. Total Environ.* **764**: 144238.
- Liu, S. M., and others. 2017. Tracing nitrogen biogeochemistry during the beginning of a spring phytoplankton bloom in the Yellow Sea using coupled nitrate nitrogen and oxygen isotope ratios. *J. Geophys. Res. Biogeo.* **122**: 2490–2508.
- Luo, L., Z. Chen, J. Lv, Y. Cheng, T. Wu, and R. Huang. 2019. Molecular understanding of dissolved black carbon sorption in soil-water environment. *Water Res.* **154**: 210–216.
- McDonough, L. K., and others. 2022. A new conceptual framework for the transformation of groundwater dissolved organic matter. *Nat. Commun.* **13**: 2153.
- Men, W., and G. Liu. 2014. Distribution of ²²⁶Ra and the residence time of the shelf water in the Yellow Sea and the East China Sea. *J. Radioanal. Nucl. Chem.* **303**: 2333–2344.
- Merder, J., and others. 2020. ICBM-OCEAN: Processing ultrahigh-resolution mass spectrometry data of complex molecular mixtures. *Anal. Chem.* **92**: 6832–6838.
- Milliman, J. D., and K. L. Farnsworth. 2011. River discharge to the Coastal Ocean—A global synthesis. Cambridge University Press.
- Mori, Y., J. Nishioka, S. Fujio, and Y. Yamashita. 2021. Transport of dissolved black carbon from marginal sea sediments to the western North Pacific. *Prog. Oceanogr.* **93**: 102552.
- Nakane, M., T. Ajioka, and Y. Yamashita. 2017. Distribution and sources of dissolved black carbon in surface waters of the Chukchi Sea, Bering Sea, and the North Pacific Ocean. *Front. Earth Sci.* **5**: 34.
- Norwood, M. J., P. Louchouart, L.-J. Kuo, and O. R. Harvey. 2013. Characterization and biodegradation of water-soluble biomarkers and organic carbon extracted from low temperature chars. *Org. Geochem.* **56**: 111–119.
- Qi, Y., and others. 2020. Dissolved black carbon is not likely a significant refractory organic carbon pool in rivers and oceans. *Nat. Commun.* **11**: 5051.
- Qi, Y., and others. 2022. Deciphering dissolved organic matter by Fourier transform ion cyclotron resonance mass spectrometry (FT-ICR MS): From bulk to fractions and individuals. *Carbon Research* **1**. doi:10.1007/s44246-44022-00002-44248
- RCoreTeam. 2022. R: A language and environment for statistical computing. R Foundation for Statistical Computing.
- Riedel, T., H. Biester, and T. Dittmar. 2012. Molecular fractionation of dissolved organic matter with metal salts. *Environ. Sci. Technol.* **46**: 4419–4426.

- Roebuck, J. A., Jr., D. C. Podgorski, S. Wagner, and R. Jaffé. 2017. Photodissolution of charcoal and fire-impacted soil as a potential source of dissolved black carbon in aquatic environments. *Org. Geochem.* **112**: 16–21.
- Schlitzer, R. 2023. Ocean data view. odv.awi.de
- Schmidt, M. W. I., and A. G. Noack. 2000. Black carbon in soils and sediments: Analysis, distribution, implications, and current challenges. *Global Biogeochem. Cy.* **14**: 777–793.
- Seidel, M., and others. 2014. Biogeochemistry of dissolved organic matter in an anoxic intertidal creek bank. *Geochim. Cosmochim. Acta* **140**: 418–434.
- Seidel, M., and others. 2015. Benthic-pelagic coupling of nutrients and dissolved organic matter composition in an intertidal sandy beach. *Mar. Chem.* **176**: 150–163.
- Stubbins, A., and others. 2010. Illuminated darkness: Molecular signatures of Congo River dissolved organic matter and its photochemical alteration as revealed by ultrahigh precision mass spectrometry. *Limnol. Oceanogr.* **55**: 1467–1477.
- Stubbins, A., J. Niggemann, and T. Dittmar. 2012. Photolability of deep ocean dissolved black carbon. *Biogeosciences* **9**: 1661–1670.
- Stubbins, A., and others. 2015. Utilizing colored dissolved organic matter to derive dissolved black carbon export by arctic rivers. *Front. Earth Sci.* **3**. doi:10.3389/feart.2015.00063
- Wagner, S., T. Riedel, J. Niggemann, A. V. Vahatalo, T. Dittmar, and R. Jaffe. 2015. Linking the molecular signature of Heteroatomic dissolved organic matter to watershed characteristics in world Rivers. *Environ. Sci. Technol.* **49**: 13798–13806.
- Wagner, S., R. Jaffé, and A. Stubbins. 2018. Dissolved black carbon in aquatic ecosystems. *Limnol. Oceanogr. Lett.* **3**: 168–185.
- Wagner, S., and others. 2019a. Isotopic composition of oceanic dissolved black carbon reveals non-riverine source. *Nat. Commun.* **10**: 5064.
- Wagner, S., Brantley, S., Stuber, S., Van Stan, J., Whitetree, A., Stubbins, A., and others. 2019b. Dissolved black carbon in throughfall and stemflow in a fire-managed longleaf pine woodland. *Biogeochemistry* **146**: 191–207.
- Wagner, S., and others. 2021. Questions remain about the biolability of dissolved black carbon along the combustion continuum. *Nat. Commun.* **12**: 4281.
- Wang, X. 2018. Combined spectrum and chromatographic technique to trace the sources, compositions and transformations of dissolved organic matter in Changjiang-East China Sea continuum. East China Normal University.
- Wang, X., C. Xu, E. M. Druffel, Y. Xue, and Y. Qi. 2016. Two black carbon pools transported by the Changjiang and Huanghe Rivers in China. *Global Biogeochem. Cy.* **30**: 1778–1790.
- Xing, J., and others. 2019. Atmospheric wet deposition of dissolved organic carbon to a typical anthropogenic-influenced semi-enclosed bay in the western Yellow Sea, China: Flux, sources and potential ecological environmental effects. *Ecotoxicol. Environ. Saf.* **182**: 109371.
- Yamashita, Y., M. Nakane, Y. Mori, J. Nishioka, and H. Ogawa. 2022. Fate of dissolved black carbon in the deep Pacific Ocean. *Nat. Commun.* **13**: 307.
- Yamashita, Y., Y. Mori, and H. Ogawa. 2023. Hydrothermal-derived black carbon as a source of recalcitrant dissolved organic carbon in the ocean. *Sci. Adv.* **9**: eade3807.
- Yu, X., F. Shen, and Y. Liu. 2016. Light absorption properties of CDOM in the Changjiang (Yangtze) estuarine and coastal waters: An alternative approach for DOC estimation. *Estuar. Coast. Shelf Sci.* **181**: 302–311.
- Zhang, R., and others. 2023. Seasonal variations in the sources and influential factors of aerosol dissolved black carbon at a southeast coastal site in China. *J. Geophys. Res. Atmos.* **128**: e2023JD038515.
- Zhao, W., H. Bao, D. Huang, J. Niggemann, T. Dittmar, and S.-J. Kao. 2023. Evidence from molecular marker and FT-ICR-MS analyses for the source and transport of dissolved black carbon under variable water discharge of a subtropical estuary. *Biogeochemistry* **162**: 43–55.
- Ziolkowski, L. A., and E. R. M. Druffel. 2010. Aged black carbon identified in marine dissolved organic carbon. *Geophys. Res. Lett.* **37**. doi:10.1029/2010GL043963

Acknowledgment

This study is funded by the National Natural Science Foundation of China (Nos: 41721005, 42076041, and 92251306), the Natural Science Foundation of Fujian Province (2020J05010), the Fundamental Research Funds for the Central Universities (20720200115). Ina Ulber and Katrin Klapproth are acknowledged for their laboratory assistance during the FT-ICR-MS and DBC_{BPCA} analysis. Dr. Hui Wu and Dr. Ergang Lian are acknowledged for helping to identify the main water masses in the study region. Dr. Hongyan Bao acknowledges Hanse-Wissenschaftskolleg (HWK) for financially supporting her stay in Germany.

Conflict of Interest

None declared.

Submitted 03 February 2023

Revised 20 July 2023

Accepted 23 September 2023

Associate editor: Elizabeth Kujawinski